TiO_2-UV detection under different types of acids and rinsing process for films preparation

Janjira Sivapatarnkun[a], Kamon Aiempanakit[a], Suriyakit Yommee[b], Sayan Pudwat[a, *]

[a] Department of Physics, Thammasat University, Pathumthani, 12120 Thailand
[b] Department of Environmental Science, Thammasat University, Pathumthani, 12120 Thailand

***Corresponding Author:** psayan@tu.ac.th
https://doi.org/10.55674/jmsae.v11i3.251924

Received: 10 March 2023 | **Revised:** 14 April 2023 | **Accepted:** 25 August 2023 | **Available online:** 1 September 2023

Abstract

Titanium dioxide (TiO_2) films were prepared by the sol–gel method under different types of acids. Effect of hydrochloric acid (HCl), nitric acid (HNO_3) and nature-based solutions (NBS) under ultraviolet (UV) detection of films were investigated. Films were coated by dip coating on glass substrate. Moreover, TiO_2 films were compared properties on water rinsing (Ri) and without rinsing (WRi) processes. The phase structure of prepared samples was characterized by means of X-ray powder diffraction (XRD). The results confirm that films were highly crystalline anatase TiO_2 and free from other phases of titanium dioxide. For the optical property, the transmittance (%T) observed sharp rise in the violet-ultraviolet transition region and a maximum transmittance of ~80%. Photocurrents were measured under UV intensity of 260 μWcm^{-2} and DC bias voltage of -20 – 20 volts (V). The results observed that currents increased as bias voltage increased. Current - Voltage (I-V) curves observed different slopes under the different of acids and rinsing process. The photocurrent of TiO_2-NBS-Ri was greater than TiO_2-HCl-WRi and TiO_2-HNO_3-WRi of 10 and 20 times; respectively. These findings suggest that the significant effect of the acid and rinsing process on crystalline, morphological, optical, and electrical properties of nanostructured TiO_2 films would be useful for applying the device in UV photoelectric detection.

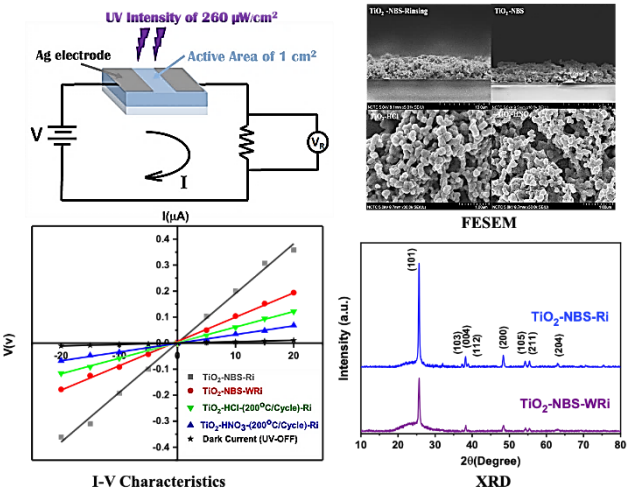

Keywords: Sol-gel; Dip coating; TiO_2 ultraviolet detection; Photoelectric property

Introduction

Detection of ultraviolet (UV) light is critical for various industrial and scientific applications, including light-wave communications, environmental monitoring, optoelectronic circuits, etc.[1]. The UV detector is outstanding performance and efficiency. Moreover, it consumes low energy with each use. Thus the cost of production is reduced even more. Wide bandgap semiconductors have been investigated for UV photodetectors due to their intrinsic visible blindness, especially metal oxide semiconductors, including TiO_2. Wide bandgap semiconductor of TiO_2 gives many excellent properties such as chemical stability, a high refractive index, and outstanding photoelectronic properties [2, 3].

Various techniques, such as electrochemical anodization [4], hydrothermal methods [5], and the sol–gel process [6], have been used to obtain high-quality TiO_2 films, which have significance for high-performance TiO_2 based photodetectors. Among these methods, the sol–gel method has the advantages of low cost and simple technology for preparing TiO_2 films.

The Sol-Gel process can be described in five steps: hydrolysis, condensation, aging, drying, and crystallization. The hydrolysis and condensation reactions are strongly affected by process parameters such as the acidity of the solution and concentration of catalysts (acid or base). The structure of the resulting gel is significantly different depending on the catalyst due to the relative rates of the hydrolysis and condensation reactions. In general, the hydrolysis step gets progressively slower under acidic

conditions. Strong acid catalysts, notably hydrochloric acid (HCl) and nitric acid (HNO_3) are used as catalysts and have significant effects on the microstructures and optical properties of TiO_2 films [7]. Therefore, these parameters under different conditions yield sol and gel with different properties and structures because the reaction rate is an important factor affecting the properties of the final product such as surface roughness film thickness particle size, etc. [8, 9]

In this work, TiO_2 films were synthesized via a simple, low-cost, chemically stable, and environmentally friendly by dip coating technique. The effect of preparing conditions on the structural, morphological, and optical properties were studied. Ag paste was used as the contact electrode to collect photocurrent for light detector that works based on the photoconductive effect. A piece of TiO_2 films and two Ohmic contacts produce a photoconductive UV detector. The coated films were characterized to study of physiochemical and UV detecting properties. The UV detecting properties were tested for films prepared with different types of acids and rinsing processes.

Materials and Methods

Films preparation

Glass substrates were first cleaned in a 5:1:1 v/v solution of deionized water, hydrogen peroxide, and ammonium hydroxide (DI:H_2O_2:NH_4OH) for 15 min at 80 ^oC. Then, the glass substrates were thoroughly rinsed with DI water and dry substrates with nitrogen (N_2) gas. Thereafter, TiO_2 sol was synthesized through a sol-gel method using titanium isopropoxide (TTIP, $Ti[OCH(CH_3)_2]_4$) as precursor and 2-propanol ($(CH_3)_2CHOH$) acts as a solvent. Briefly, the TTIP of 1 ml was dissolved in 10 ml of 2-propanol. The solution was vigorously stirred for 2 h in order to form sols. HCl and HNO_3 were used to adjust the pH of 2. The mixture of these solutions was stirred for 2 h. After aging for 24 h, the sols were transformed into gels. TiO_2 films were coated on glass substrate using dip coating method. To coat films, glass substrates were immersed vertically within the prepared solution for 5 min. After 5 min, substrates were removed from the solution and dried for 5 min with the help of drier. This completes one cycle of coating and after coating, films were rinsed (Ri) with DI water or without rinsed (WRi). The different method of drying was investigated. After each layer coating sol-gel layers were dried at 200 °C for 5 min and cooled down to temperature of air (25°C), and then the next layer was coated. These films were respectively abbreviated as TiO_2 (TiO_2≡ titanium dioxide) - NBS (NBS≡ nature-based solutions)-Ri (Ri≡ rinsing process), TiO_2-NBS-WRi (WRi≡ without rinsing process), TiO_2-HCl (HCl≡ hydrochloric acid)-Ri, TiO_2-HCl-WRi, TiO_2-HNO_3 (HNO_3≡ nitric acid)-Ri, TiO_2-HNO_3-WRi, TiO_2-HCl-(25^{o}C/Cycle)-(200 ^{o}C/Cycle)-Ri, TiO_2-HCl-(200 ^{o}C/Cycle)-Ri , and TiO_2-HNO_3-(200 ^{o}C/Cycle)-Ri. All samples were annealed temperature in air at 500^o C and annealed time of 2 h to improve crystallinity. The films were fabricated by painting Ag paste, the active area of the films was 1 cm^2. The black light F10T8BL was used as a source of UVA with a wavelength in the range of 320 – 400 nm for the central wavelength of 365 nm and UV detecting properties were studied by fabricated films.

Samples characterization

The crystal structure of the films was examined by the Bruker D2 X-ray powder diffractometer (XRD). The transmittance spectra were measured on a Thermo Scientific Genesys 10S UV-Visible Spectrophotometers. The surface morphology of the films was observed using a Hitachi SU-8030 field emission scanning electron microscope (FESEM). The current-voltage (I-V) characteristics of the films were measured using a digital multimeter PICOTEST together with a UV lamp.

Results and Discussions

The X-ray diffraction patterns of coated samples are observed in Fig. 1 (a) – (c). The XRD results in the range of 10° – 80° of the TiO_2 films annealed at 500°C on glass substrates. The XRD patterns match well with JCPDS (no.21-1272). The detected diffraction peaks centered at 25.30°, 38.10°, 48°, 54°, 55°, 63°, 69°, and 71° are corresponding to (101), (004), (200), (105), (211), (204), (116), and (220); respectively. They are well indexed to the tetragonal crystal planes of the standard anatase phase of TiO_2 structure. The films are polycrystalline in nature and show preferred orientation along (101) plane. They are observed that the coated films show anatase phase and no peaks corresponding to rutile and brookite phases, and there are no other impurity peaks, which shows clearly that TiO_2 film was well synthesized. The change in the rinsing process and types of acids affects on the intensity of peaks [10, 11]. The intensity goes on increasing as rinsing process (Ri) and decreases under without rinsing process (WRi), because film thickness of Ri increases but WRi thickness decreases. With different kinds of acids, the diffraction peaks shifted slightly to the higher angle side. The peak shift might be caused by strain that evolved in the TiO_2 nanoparticles [12]. This result

demonstrated that the sample crystallinity was a significant structure. An electron from the valence band to the conduction band corresponds to the UV absorption below 384 nm of the TiO_2 anatase phase, which corresponds to a band gap energy of 3.22 eV [13]. That mean, anatase phase with high UV absorption produce high photocurrent under driving potential.

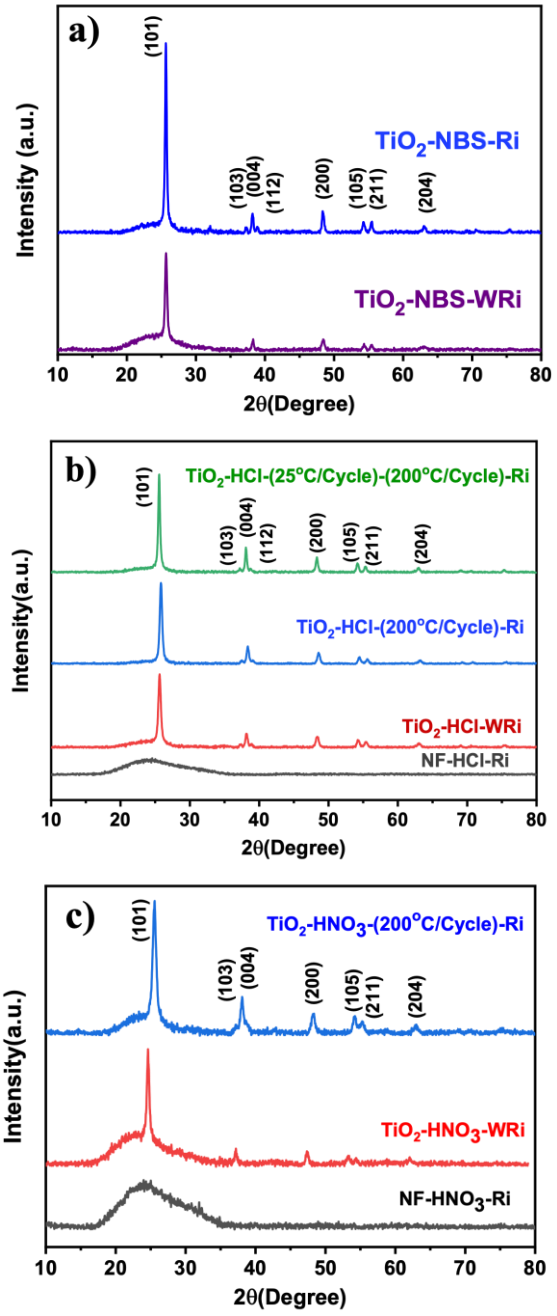

Fig. 1 XRD patterns for TiO_2 films (a) NBS-(Ri, WRi), (b) HCl-(25 °C/Cycle)-(200 °C/Cycle)-Ri, HCl-(200 °C/Cycle)-Ri, HCl-(WRi, Ri), and (c) HNO_3-(200 °C/Cycle)-Ri, HNO_3-(WRi, Ri).

The FESEM image presented in Fig. 2. The difference for each condition were (a) TiO_2- NBS-Ri, (b) TiO_2-NBS-WRi, (c)TiO_2-HCl-WRi, (d)TiO_2-HNO_3-WRi, (e)TiO_2-HCl-(200°C/Cycle)-Ri, and (f) TiO_2-HNO_3-(200°C/Cycle)-Ri. The average thickness for Fig. 2(a) and Fig. 2(b) were 3.60 μm and 1.90 μm; respectively. The microstructure can be deduced from the image brightness by superimposing the sponge-like films. Fig. 2(a) – (d) observed the sponge-like and knobs-like morphology of the titania nanostructures. The acids of the solution affect the agglomeration of the particles [14]. Fig. 2(c) and Fig. 2(d) observed that particle size decreases due to different types of acids. The structure was formed by single nano-sized titania particles linked together, resulting in a random arrangement of holes and cavities. The pores were merged, forming bigger holes with irregular shapes. The Fig. 2(e) – (f) observed the microstructures of the samples after being dried at 200 °C and annealed at 500 °C. Fig. 2(e) observed continuous films and line of traces while Fig. 2(f) observed surface cracking of TiO_2 films. Microstructure of films that observed in Fig.2 were taken different electron motion under driving potential with UV irradiation.

The UV–Vis optical transmittance spectra of TiO_2 films prepared under different conditions and annealed at 500 °C are observed in Fig. 3(a) – (c). The optical transmittance spectra were collected wavelength in the range of 200 – 1100 nm. The measurements were taken at a normal incidence using a reference glass substrate. The samples of TiO_2-NBS-Ri, TiO_2-NBS-WRi, TiO_2-HCl-Ri, TiO_2-HCl-WRi, TiO_2-HNO_3-Ri, TiO_2-HNO_3-WRi, TiO_2-HCl-(25°C/Cycle) -(200 °C/Cycle)-Ri, TiO_2-HCl-(200°C/Cycle)-Ri, and TiO_2-HNO_3-(200 °C/Cycle)-Ri observed sharp rise in transmittance at the violet-ultraviolet transition region from almost zero to maximum ~80%. The average value of transmittance for these films were around 40 – 80% in the visible region. The samples of TiO_2-NBS-Ri and TiO_2-NBS-WRi observe very low transmittance (<1%) throughout the scan range. The various measurements in sensing detection for evaluating the optical performance of conducting oxide films involved the determination of the transmittance. This behavior was attributed to increase the thickness with the number of atoms layer, that lead to increase the collisions of electromagnetic wave of light to atoms, leading to a decrease in transmittance. [15].

Fig. 4(a) – (c) observed the current (I)-voltage (V) relation under UV irradiation. Results observed an increasing trend in current with an increase in bias voltage (-20 – 20 V) for all the films and verified the contact ohmic

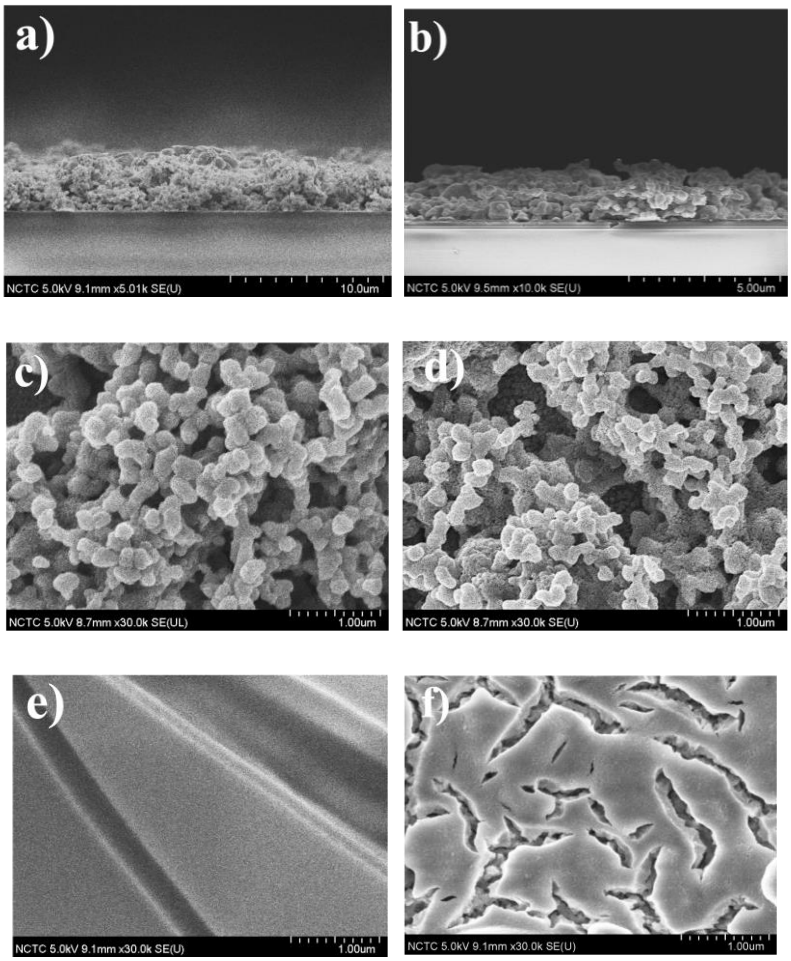

Fig. 2 Cross-section and top-view of FESEM images for the TiO_2 films (a) NBS-Ri, (b) NBS-WRi, (c) HCl-WRi, (d) HNO_3-WRi, (e) HCl-(200ºC/Cycle)-Ri, and (f) HNO_3-(200ºC/Cycle)-Ri.

nature. Fig. 4(a) is observe the I-V characteristics with various conditions of the rinsing process and different types of acids of TiO_2 films measured under UV irradiation. High-energy photons were absorbed by the TiO_2 film when light strikes the TiO_2 UV detector. A photocurrent will be observed at an exact bias voltage as photon-generated carriers drift toward the contact electrodes. Results observed that the obtained TiO_2 structure exhibits excellent ohmic behavior as indicated by a linear I-V curve dependence. Currents increase as bias voltage increases, and various conditions resulted in different slopes for I-V curves.

According to the I-V curve measurement, the photocurrent of the film rinsed was significantly higher than the film without rinsing. The photocurrent for the TiO_2-NBS-Ri and TiO_2 - NBS-WRi were 0.36 and 0.19 µA, respectively. Results of a photoconductive UV detector were on exhibit as linear I-V curves in Fig. 4(a) – (c). This result observed the high sensitivity of the TiO_2 UV detector that was obtained. Prepared TiO_2 was n-type semiconductor material with electrons as majority charge carriers. The primary cause for the photoconductive characteristics of the fabricated device is the adsorption and desorption of oxygen molecules on the surface of the TiO_2 material. On the surface of semiconductor materials, atmospheric oxygen is adsorbed, trapping electrons from its conduction band, and it is provided as eq. (1);

$$\left[O_2(\text{gas}) + e^- \rightarrow O_2^-(\text{ads})\right] \quad (1)$$

Electron-hole pairs are generated as photons with energies higher than the band gap are incident on the material when semiconductor material is exposed to UV light. As shown in eq. (2) these photogenerated holes recombine with the adsorbed oxygen to desorb oxygen from the surface of the semiconductor material.

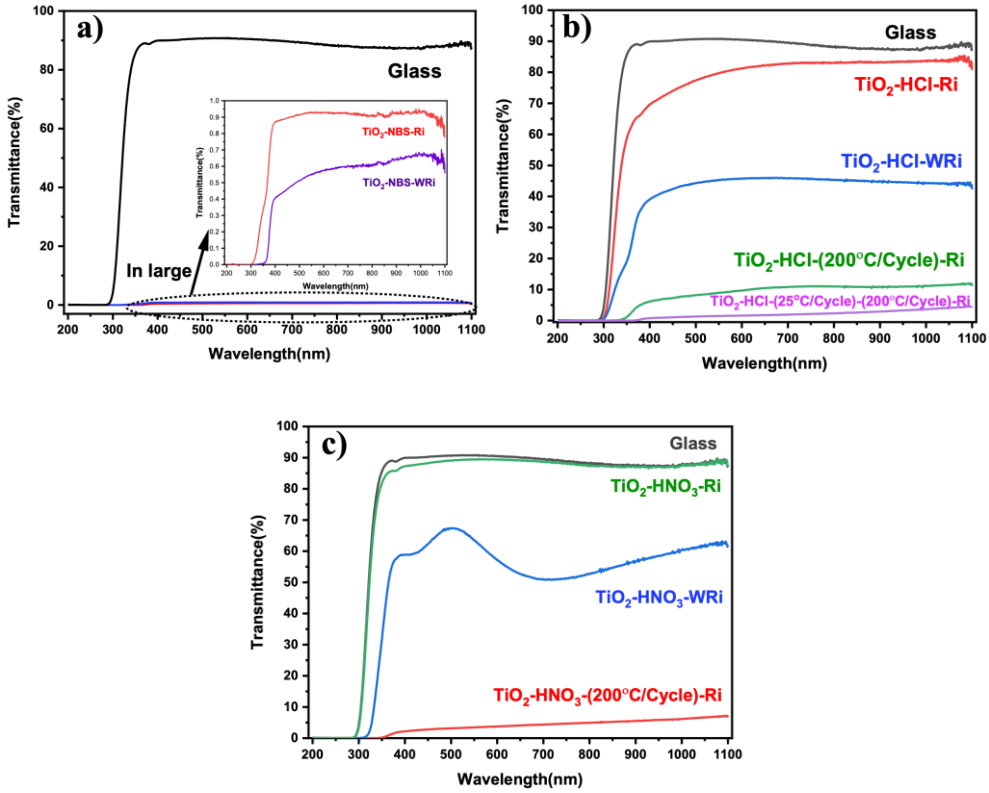

Fig. 3 Transmittance spectra of the TiO_2 films (a) NBS-(Ri,WRi), (b) HCl-(Ri,WRi), HCl-(200 ºC/Cycle)-Ri and HCl-(25ºC/Cycle)-(200 ºC/Cycle)-Ri, and (c) HNO_3-(Ri,WRi) and HNO_3-(200 ºC/Cycle)-Ri.

$$\left[h^+ + O_2^- (ads) \rightarrow O_2 (gas) \right] \quad (2)$$

This process generates to increase carrier concentration, which causes increasing photocurrent when exposed to UV light. Even after the UV light is turned off, photocurrent can be observed flowing through the device. This is a result of the persistent photoconductive (PPC) phenomenon, in which photoinduced current persisted in the device even after the light source is turned off. As a result, the photocurrent does not return to its initial value when the UV lamp is turned off. The time period photoconduction process depends on surface-related oxygen adsorption and photodesorption processes of that relates to the PPC effect [16 – 18].

Fig. 4(b) and (c) the photocurrent of the different types of acid-adjusted samples after being dried at 200 °C and annealed at 500 °C. The photocurrent for the TiO_2-HCl-Ri and TiO_2-HCl-(200ºC/Cycle)-Ri for potential different of -20 – 20V were 0.01 and 0.12 µA, respectively. Types of acid enhanced the crystallinity also promotes the formation of crystallite size. Such results observe that the fabricated devices were gotten internal gain. It was conceivable that the TiO_2 defects on the surface acted as trapped states that captured photoelectrons under irradiation. The trapped states enhanced the carrier lifetime and increased internal gain of device by decreasing the likelihood of electron-hole pair recombination [19, 20].

In addition, repeatability is also one important parameter that can be used to evaluate the reliability of a fabricated detector. The repeatability of the detector was investigated by testing three conditions as observed in Fig. 5(a) and (b). The photocurrent in continuous seven test days indicates repeatability. The average response value had a small relative deviation, revealing that the detector maintains its initial response without significant decreasing. Moreover, the long-term stability of a UV detector has attained much attention, for which the reliability of UV detectors. To verify the stability of the detector, the UV responses observed the photocurrent over 7 days were tested at room temperature.

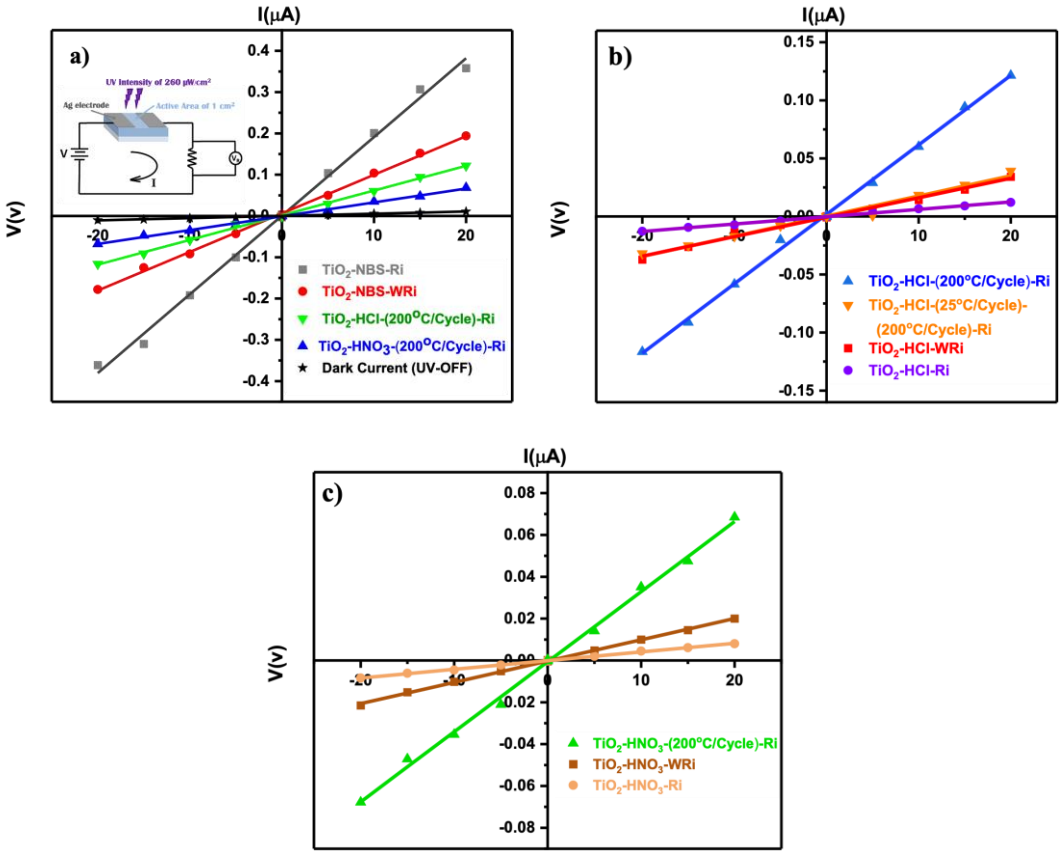

Fig. 4 The I–V characteristics of the samples under UV illumination, the inset shows the testing circuit (a) NBS-(Ri, WRi), (HCl, HNO_3)-(200 ºC/ Cycle)-Ri and Darkness, (b) HCl-(200 ºC/ Cycle)-Ri, HCl-(25ºC/ Cycle)-(200 ºC/ Cycle)-Ri, HCl-(WRi, Ri), and (c) HNO_3-(200 ºC/Cycle)-Ri and HNO_3-(WRi, Ri).

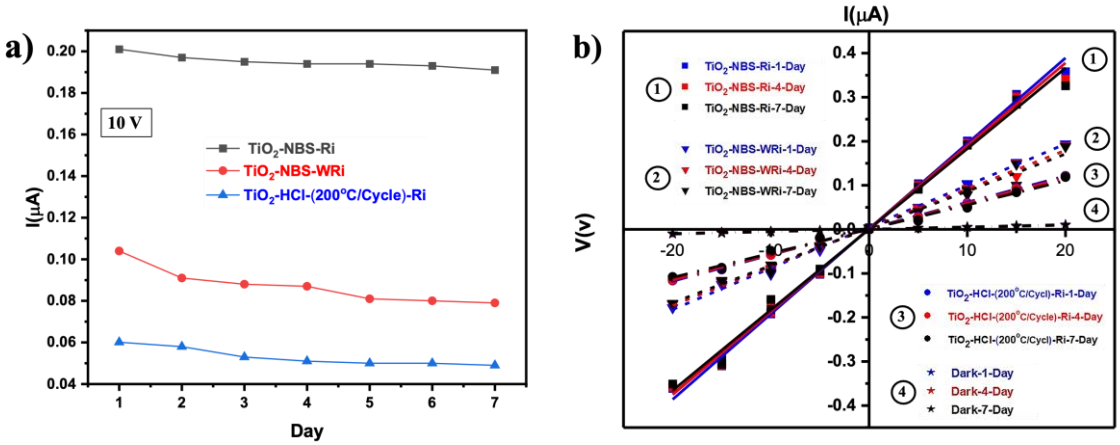

Fig. 5 Repeatability of the UV detector (a) NBS - (Ri, WRi) and HCl-(200 ºC/ Cycle)-Ri, (b) NBS-Ri-(1, 4, 7)-Day, NBS-WRi-(1, 4, 7)-Day, HCl-(200ºC/Cycle)-Ri-(1, 4, 7)-Day and Dark-(1, 4, 7)-Day.

Conclusion

TiO_2-based UV detector had been successfully prepared by using TiO_2 films coated via a simple and low-cost by dip coating technique. TiO_2-films UV detectors with Ag electrodes were fabricated. The photoelectrical observation measured that the TiO_2-NBS-Ri photocurrent was 30 and 45 times higher than the TiO_2-HCl-Ri and TiO_2-HNO_3-Ri and the resistance under UV illumination of the TiO_2-NBS-Ri was less than the TiO_2-NBS-WRi. The UV detector based on TiO_2-NBS-Ri exhibits high performance including the preferable response and good repeatability. All of these results observe that these films can be a promising candidate as a UV photodetector applications.

Acknowledgement

The authors would like to thank Thammasat University for funding, research facilities, and Innovative sensor and nano-Electronic Devices (ISED-TU).

References

[1] D. Zhang, F. Jing, F. Gao, L. Shen, D. Sun, J. Zhou, Y. Chen, S. Ruan, Enhanced performance of a TiO_2 ultraviolet detector modified with graphene oxide, RSC Adv. 5(102) (2015) 83795 – 83800.

[2] K. LV, M. Zhang, C. Liu, G. Liu, H. Li, S. Wen, Y. Chen, S. Ruan, TiO_2 ultraviolet detector based on LaAlO3 substrate with low dark current, J. Alloys Compd. 580(2013) 614 – 617.

[3] P. Parthasarathy, Synthesis and UV detection characteristics of TiO_2 thin film prepared through sol gel route, IOP Conf. Ser. :Mater. Sci. Eng. 360(1) (2018) 012056.

[4] J. Zou, Q. Zhang, K. Huang, N. Marzari, Ultraviolet photodetectors based on anodic TiO2 nanotube arrays, J. Phys. Chem. C. 114(24) (2010) 0725 – 10729.

[5] Y. Han, G. Wu, M. Wang, H. Chen, Hybrid ultraviolet photodetectors with high photosensitivity based on TiO_2 nanorods array and polyfluorene, Appl. Surf. Sci. 256(5) (2009) 1530 – 1533.

[6] H. Xue, X. Kong, Z. Liu, C. Liu, J. Zhou, W. Chen, Q. Xu, TiO_2 based metal-semiconductor-metal ultraviolet photodetectors, Appl. Phys. Lett. 90(20) (2007) 201118.

[7] J. Zhou, B. Song, G. Zhao, G. Han, Effects of acid on the microstructures and properties of three-dimensional TiO_2 hierarchical structures by solvothermal method, Nanoscale research letters, 7(1) (2012) 1 – 10.

[8] C. J. Brinker, G. W. Scherer, Sol-gel science: the physics and chemistry of sol-gel processing, Academic press, 2013.

[9] H. M. Shang, Y. Wang, S. J. Limmer, T. P. Chou, K. Takahashi, G.Z. Cao, Optically transparent superhydrophobic silica-based films, Thin Solid Films, 472(1-2) (2005) 37 – 43.

[10] B. Tryba, M. Tygielska, C. Colbeau-Justin, E, Kusiak-Nejman, J. Kapica-Kozar, R. Wróbel, N. Guskos, Influence of pH of sol-gel solution on phase composition and photocatalytic activity of TiO_2 under UV and visible light, Mater. Res. Bull. 84 (2016) 152 – 161.

[11] J. Zhou, B. Song, G. Zhao, G. Han, Effects of acid on the microstructures and properties of three-dimensional TiO_2 hierarchical structures by solvothermal method, Nanoscale research letters, 7(1) (2012) 1 – 10.

[12] M. Tsega, F. Dejene, Influence of acidic pH on the formulation of TiO_2 nanocrystalline powders with enhanced photoluminescence property, Heliyon. 3(2) (2017) e00246.

[13] S. Mondal, D. Basak, Very high photoresponse towards low-powered UV light under low-biased condition by nanocrystal assembled TiO_2 film, Appl. Surf. Sci. 427(2018) 814 – 822.

[14] I. S. Aida, S. Sreekantan, Effect of pH on TiO_2 nanoparticles via sol-gel method, Adv. Mat. Res. 173 (2011) 184 – 189.

[15] W. Langel, P. Y. Yu, M. Cardona, Fundamentals of semiconductors physics and materials properties, 3rd rev. and enlarged edn. (Advanced texts in physics) (2003) 729 – 730.

[16] S. Chang, M. Park, Q. Kuang, Y. Deng, A. Sood, D. Polla, Z. Wang, Giant enhancement in UV response of ZnO nanobelts by polymer surface-functionalization, J. Am. Chem. Soc. 129(40) (2007) 12096 - 12097.

[17] J. Wang, X. Nie, W. Wang, Z. Zhao, L. Li, Z. Zhang, Single-layer graphene-TiO_2 nanotubes array heterojunction as photoanode to enhance the photoelectric of DSSCs, Optik. 242 (2021) 167245.

[18] D. Chen, Y. J. Yuan, Thin-film sensors for detection of formaldehyde: A review, IEEE Sens. J. 15(12) (2015) 6749 – 6760.

[19] L. Wang, W. Yang, H. Chong, L. Wang, F. Gao, L. Tian, Z. Yang, Efficient ultraviolet photodetectors based on TiO_2 nanotube arrays with tailored structures, RSC Adv. 5(65) (2015) 52388 - 52394.

[20] D. Nunes, A. Pimentel, A. Araujo, T. Calmeiro, S. Panigrahi, J. Pinto, P. Barquinha, M. Gama, E.

Fortunato, R. Martins, Enhanced UV flexible photodetectors and photocatalysts based on TiO_2 nanoplatforms, Top Catal. 61(15) (2018) 1591 - 1606.

[21] J. Zou, Q. Zhang, K. Huang, N. Marzari, Ultraviolet photodetectors based on anodic TiO_2 nanotube arrays, J. Phys. Chem. 114(24) (2010) 10725 – 10729.

[22] H. Liu, W. Lin, W. Sun, S. Wei, S. Yu, A study of ultrasonic spray pyrolysis deposited rutile-TiO_2-based metal-semiconductor-metal ultraviolet photodetector, Mater. Sci. Semicond. Process. 57 (2017) 90 – 94.

[23] K. Chahrour, F. Yam, R. Abdalrheem, High-performance UV photodetector of anodic rutile TiO_2 nanotube arrays, Mater. Lett. 248 (2019) 161 – 164.